Version of record at: https://doi.org/10.1016/j.celrep.2021.109753

Article

Cell Reports

Vitamin B_{12} impacts amyloid beta-induced proteotoxicity by regulating the methionine/S-adenosylmethionine cycle

Graphical abstract

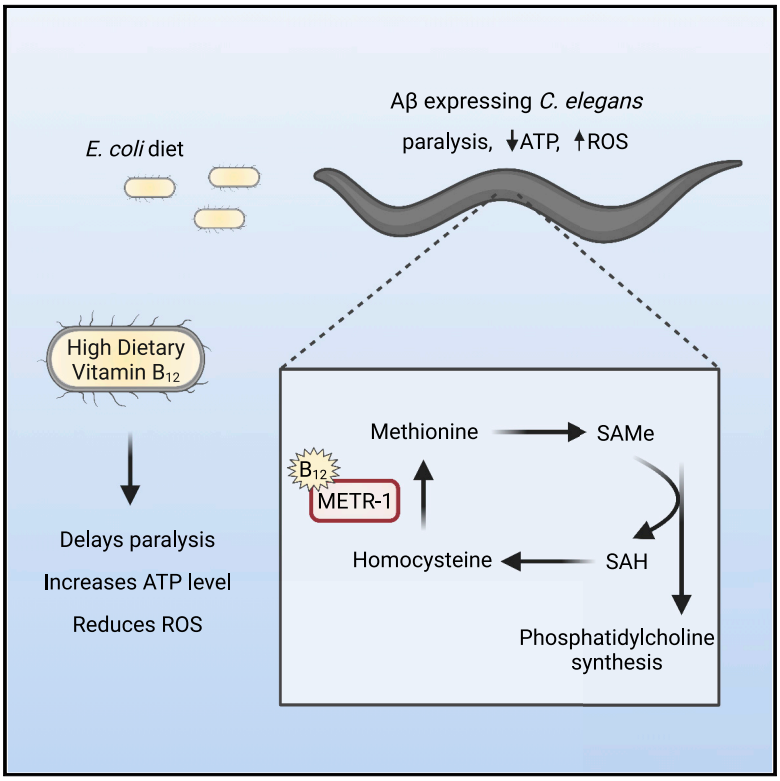

Highlights

- Dietary vitamin B_{12} reduces the proteotoxic effects of Aβ in *C. elegans*
- Vitamin B_{12} is protective even when given to deficient worms only during adulthood
- B_{12} has this impact by acting in *C. elegans* as a cofactor for methionine synthase

Authors

Andy B. Lam, Kirsten Kervin, Jessica E. Tanis

Correspondence

jtanis@udel.edu

In brief

Lam et al. discover that feeding a vitamin-B_{12}-deficient diet to amyloid beta (Aβ)-expressing *C. elegans* accelerates paralysis, reduces ATP levels, and increases oxidative stress. Their results indicate that vitamin B_{12} affects the methionine/SAMe cycle to protect against Aβ-induced proteotoxicity.

Lam et al., 2021, Cell Reports *36*, 109753
September 28, 2021
https://doi.org/10.1016/j.celrep.2021.109753

Version of record at: https://doi.org/10.1016/j.celrep.2021.109753

Cell Reports

CellPress
OPEN ACCESS

Article

Vitamin B_{12} impacts amyloid beta-induced proteotoxicity by regulating the methionine/S-adenosylmethionine cycle

Andy B. Lam,[1] Kirsten Kervin,[1] and Jessica E. Tanis[1,2,*]
[1]Department of Biological Sciences, University of Delaware, Newark, DE 19716, USA
[2]Lead contact
*Correspondence: jtanis@udel.edu
https://doi.org/10.1016/j.celrep.2021.109753

SUMMARY

Alzheimer's disease (AD) is a devastating neurodegenerative disorder with no effective treatment. Diet, as a modifiable risk factor for AD, could potentially be targeted to slow disease onset and progression. However, complexity of the human diet and indirect effects of the microbiome make it challenging to identify protective nutrients. Multiple factors contribute to AD pathogenesis, including amyloid beta (Aβ) deposition, energy crisis, and oxidative stress. Here, we use *Caenorhabditis elegans* to define the impact of diet on Aβ proteotoxicity. We discover that dietary vitamin B_{12} alleviates mitochondrial fragmentation, bioenergetic defects, and oxidative stress, delaying Aβ-induced paralysis without affecting Aβ accumulation. Vitamin B_{12} has this protective effect by acting as a cofactor for methionine synthase, impacting the methionine/S-adenosylmethionine (SAMe) cycle. Vitamin B_{12} supplementation of B_{12}-deficient adult Aβ animals is beneficial, demonstrating potential for vitamin B_{12} as a therapy to target pathogenic features of AD triggered by proteotoxic stress.

INTRODUCTION

Alzheimer's disease (AD), the most common cause of dementia, is a multifactorial neurodegenerative disorder characterized by accumulation of amyloid beta (Aβ) plaques, hyperphosphorylated tau, oxidative stress, mitochondrial defects, and impaired glucose metabolism (Butterfield and Halliwell, 2019; Chakravorty et al., 2019; Lin and Beal, 2006; Long and Holtzman, 2019). Some AD risk factors, including genetic predisposition and aging, are nonmodifiable, while other risk factors, such as diet, can be altered to impact disease onset and progression (Thelen and Brown-Borg, 2020). Complex diets consist of macronutrients, including carbohydrates, fats, and proteins, as well as vitamin and mineral micronutrients. It is challenging to determine which individual nutrients are neuroprotective in humans as well as other mammals due to organismal complexity, genetic diversity, and consumption of complex diets. Indirect dietary effects of gut microbiota, which provide micronutrients to the host, further complicate studies.

Caenorhabditis elegans eat a simple diet of *E. coli* in the laboratory, and consumption of different bacterial strains affects nematode gene expression, metabolic profile, development, fertility, and fat storage (Brooks et al., 2009; Cabreiro et al., 2013; Cogliati et al., 2020; Han et al., 2017; MacNeil et al., 2013; Revtovich et al., 2019; Virk et al., 2012, 2016; Watson et al., 2014). With its genetic tools and short lifespan, *C. elegans* is an ideal system for the study of age-related diseases and has been used extensively to identify factors that influence Aβ proteotoxicity (Fang et al., 2019; Han et al., 2017; Hassan et al., 2015; Lublin and Link, 2013; Sorrentino et al., 2017; Teo et al., 2019). Transgenic expression of toxic human Aβ peptides in *C. elegans* body wall muscles generates robust time-dependent paralysis as well as AD-like pathological features, including defects in mitochondrial morphology, reduced ATP levels, and oxidative stress (Drake et al., 2003; Fonte et al., 2011; Link, 1995; McColl et al., 2012; Sorrentino et al., 2017). Our goal was to use *C. elegans* to define the impact of diet on Aβ-induced proteotoxicity.

We discovered that Aβ-expressing *C. elegans* fed HB101 *E. coli* exhibited delayed paralysis, higher ATP levels, decreased mitochondrial fragmentation, and reduced reactive oxygen species (ROS) compared to those raised on OP50 *E. coli*. Mild vitamin B_{12} deficiency was observed in animals grown on OP50, but not HB101. B_{12} supplementation delayed Aβ-induced paralysis and protected against the increase in ROS and energy crisis observed in animals fed OP50 but did not have additive beneficial impact on those that consumed HB101. The protective effects of vitamin B_{12} required methionine synthase, indicating function as an enzyme cofactor rather than an antioxidant, and the methionine/S-adenosylmethionine (SAMe) cycle. Vitamin B_{12} supplementation in adulthood was beneficial for B_{12}-deficient *C. elegans*, suggesting that administration even late in life has potential as a therapeutic intervention.

RESULTS

Diet alters Aβ-induced paralysis in *C. elegans*

Genetic evidence suggests that Aβ-induced proteotoxicity is a causal factor in AD development (Chartier-Harlin et al., 1991;

Version of record at: https://doi.org/10.1016/j.celrep.2021.109753

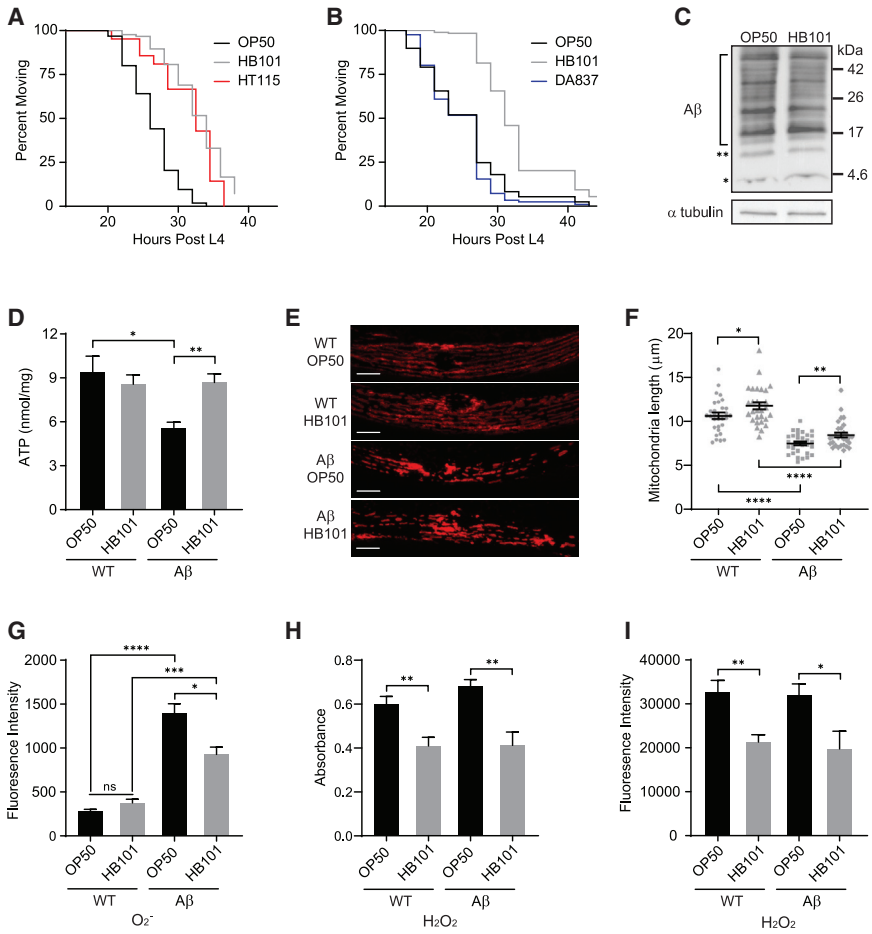

Figure 1. Diet impacts Aβ-induced paralysis, energy availability, oxidative stress, and mitochondrial morphology without altering Aβ accumulation

(A) Aβ animals fed HB101 (gray) and HT115 (red) exhibited delayed paralysis compared to those on OP50 (black) ($n \geq 89$).

(B) Aβ animals fed DA837 (blue) and OP50 (black) became paralyzed at the same time ($n \geq 183$).

(C) Western analysis showed no effect of diet on Aβ accumulation. The Aβ monomer and dimer are indicated by asterisks (* and **, respectively); bracket shows Aβ oligomers. Additional replicates are in Figure S1F.

(D) ATP levels in Aβ *C. elegans* fed OP50 were reduced compared to wild type (WT); the HB101 diet increased ATP in Aβ animals ($n \geq 10$).

(E) Representative images of mitochondria, visualized with TOMM-20::RFP, in WT and Aβ animals. Scale bars, 10 μm.

(F) Average mitochondrial length was affected by Aβ accumulation and diet; individual measurements (gray symbols, $n \geq 30$) indicated.

(G) Superoxide (O_2^-), measured with MitoSox, was higher in Aβ animals fed OP50 versus HB101 ($n \geq 11$).

(H) Hydrogen peroxide (H_2O_2) level, quantified with Amplex red, was greater in both WT and Aβ nematodes given OP50 ($n \geq 7$).

(I) H_2O_2, measured with H_2DCFDA, was increased in WT and Aβ animals fed OP50 ($n \geq 8$).

Error bars show SEM; *$p < 0.05$, **$p < 0.01$, and ***$p < 0.001$, one-way ANOVA with Dunnett's post-test. See also Figures S1 and S2.

Goate et al., 1991; Long and Holtzman, 2019). Little correlation between the density of extracellular Aβ plaques and AD severity (Chen et al., 2017; De Strooper and Karran, 2016) suggests that the toxic effects likely result from small soluble Aβ oligomers, which can enter lipid bilayers (Cline et al., 2018; Pagani and Eckert, 2011). Transgenic expression of human $A\beta^{1-42}$ in *C. elegans* muscles causes AD-like cellular abnormalities, including reduced ATP levels, defects in mitochondrial morphology, and oxidative stress, as well as robust time-dependent paralysis (Drake et al., 2003; Fonte et al., 2011; McColl et al., 2012). Altered time to paralysis has been used extensively to identify genes and pharmacological agents that influence Aβ-induced proteotoxicity (Cacho-Valadez et al., 2012; Han et al., 2017; Hassan et al., 2015; Lublin and Link, 2013; Sorrentino et al., 2017). While investigating the impact of genetic factors on Aβ-induced paralysis, we noticed that animals fed OP50 B-type *E. coli* consistently paralyzed faster than those given HT115(DE3), an RNase-III-deficient K12-derived *E. coli* used for RNA interference experiments. To determine if diet was impacting Aβ proteotoxicity, we raised Aβ animals on different *E. coli* diets and discovered that those fed HT115 or HB101, a B × K12 hybrid, exhibited a significant delay in paralysis compared to those that consumed OP50 (Figures 1A, S1A, and S1B).

Since caloric restriction reduces Aβ toxicity (Steinkraus et al., 2008), we first sought to determine if the altered time to paralysis was due to differences in bacterial growth or *C. elegans* feeding. We found no difference in bacterial concentration on OP50 and HB101 plates (Figure S1C) or pharyngeal pumping rates (Figure S1D) in *C. elegans* grown on the different diets. Aβ animals fed DA837, another *E. coli* B strain that is hard for worms to ingest (Shtonda and Avery, 2006), exhibited paralysis indistinguishable from those given OP50 (Figures 1B and S1A). Finally, the HB101 diet was still protective in an *eat-2* mutant, which exhibits delayed Aβ-induced paralysis due to dietary restriction (Figure S1E; Steinkraus et al. 2008). Together, these results suggest that the diet-induced shift in paralysis was not due to changes in ingestion or dietary restriction.

Reducing Aβ levels delays paralysis (Sorrentino et al., 2017), so we next sought to establish if diet impacted Aβ content. We observed no difference in Aβ accumulation between animals raised on OP50 and HB101 using immunoblotting (Figures 1C and S1F). Through a genetic approach, we found that *pek-1(ok275)* and *gcn-2(ok871)*, which alter protein synthesis (Baker et al., 2012; Rousakis et al., 2013; Shen et al., 2005), did not impact the HB101 protective effect (Figures S1G and S1H).

Version of record at: https://doi.org/10.1016/j.celrep.2021.109753

CellPress
OPEN ACCESS

Our results suggest that the HB101 diet delays Aβ-induced paralysis without affecting Aβ accumulation.

Diet impacts ATP levels, mitochondrial morphology, and ROS in Aβ animals

Bioenergetic deficits, which cause synaptic dysfunction in AD individuals, are exacerbated by Aβ accumulation (Chakravorty et al., 2019). *C. elegans* expressing Aβ exhibit a decrease in ATP levels and defects in electron transport chain complex activity, indicating that energy crisis is a fundamental consequence of Aβ buildup (Fang et al., 2019; Fong et al., 2016; Sorrentino et al., 2017; Teo et al., 2019). Therefore, we tested the impact of diet on ATP levels and found that Aβ animals fed HB101 had significantly higher ATP compared to those on OP50 (Figure 1D). Diet had no effect on ATP levels in wild-type *C. elegans* (Figure 1D), indicating that the dietary protection was only required for animals under proteotoxic stress.

To elucidate the mechanism underlying the diet-induced change in ATP level, we assessed mitochondrial gene transcripts, protein levels, morphology, and respiration activity. Transcript levels of genes required for oxidative phosphorylation (Figure S2A) and mitochondrial protein content (Figures S2B and S2C) were unchanged between Aβ animals fed different diets. Aβ expression disrupts mitochondrial network integrity, which is important for bioenergetic efficiency (Figure 1E; Fonte et al., 2011; Sorrentino et al., 2017). *C. elegans* muscle mitochondria are arranged in a periodic pattern that can be visualized with red fluorescent protein (RFP)-tagged TOMM-20 (Wei and Ruvkun, 2020). We quantified mitochondria length and found that the HB101 diet reduced fragmentation in both wild-type and Aβ animals (Figure 1F). To assess if these changes in mitochondrial morphology impacted cellular respiration, we used a Seahorse XFe96 Analyzer. Aβ expression caused a significant change in basal respiration rate, maximal respiration rate, and spare respiratory capacity; however, diet did not alter mitochondrial respiration in either wild-type or Aβ nematodes (Figures S2D–S2F). While it remains possible that the severe mitochondrial fragmentation in Aβ animals alters respiration, the dietary impact on morphology did not change mitochondrial function. Instead, diet likely affects ATP levels by altering glycolytic output or energy expenditure.

Aβ accumulation promotes production of ROS including superoxide (O_2^-) and hydrogen peroxide (H_2O_2). Oxidative stress, stemming from an imbalance between ROS formation and antioxidant defenses, plays a causal role in AD pathogenesis (Butterfield and Halliwell, 2019; Drake et al., 2003; Wang et al., 2014). Therefore, we investigated the impact of Aβ and diet on O_2^- and H_2O_2 levels using ROS indicators. Expression of Aβ resulted in a substantial increase in O_2^-, but Aβ animals fed HB101 had significantly reduced O_2^- levels compared to those raised on OP50 (Figure 1G). Both wild-type and Aβ *C. elegans* raised on OP50 exhibited significantly higher H_2O_2 than those on HB101 (Figures 1H and 1I). In conclusion, diet impacts ATP level, mitochondrial fragmentation, and ROS accumulation in Aβ-expressing *C. elegans*.

Vitamin B_{12} protects against Aβ-induced paralysis and energy deficits

OP50 and HB101 differ in carbohydrate content and fatty acid composition (Brooks et al., 2009; Neve et al., 2020; Revtovich et al., 2019). Thus, we considered whether differences in macronutrients could alter the paralysis of Aβ worms. Supplementation of plates with glucose (Figures 2A and S3A) or oleic acid (Figures 2B, S3A, and S3B) did not eliminate the dietary shift in Aβ-induced paralysis, suggesting that these macronutrients are not responsible for the impact of diet. However, Aβ animals raised on OP50 supplemented with glucose paralyzed significantly faster than those fed OP50 alone, consistent with reports of excess glucose shortening lifespan (Lee et al., 2009; Schulz et al., 2007). Supplementation of HB101 plates with glucose had no effect (Figures 2A and S3A), suggesting that the nutrient in HB101 that protects against Aβ proteotoxicity may also defend against the detrimental consequences of high glucose.

E. coli strains also differ in micronutrient content and *C. elegans,* like humans, must obtain several essential vitamins from their diet. Mild vitamin B_{12} deficiency is observed in animals fed OP50, which has reduced expression of the *tonB* transporter that mediates B_{12} uptake (Revtovich et al., 2019; Watson et al., 2014). *C. elegans* vitamin B_{12} status can be assessed using a *Pacdh-1*::GFP reporter, which is expressed in response to propionic acid accumulation resulting from B_{12} deficiency (MacNeil et al., 2013; Revtovich et al., 2019; Watson et al., 2014, 2016; Wei and Ruvkun, 2020). GFP was highly expressed in animals grown on OP50 and DA837, the diets that led to faster paralysis of Aβ worms, and B_{12} supplementation suppressed GFP expression (Figure 2C). In contrast, GFP expression was repressed in *C. elegans* raised on the HB101 and HT115 protective diets, suggesting high B_{12} levels (Figure 2C). Supplementation of OP50 plates with 148 nM vitamin B_{12} eliminated the dietary shift in Aβ-induced paralysis (Figure 2D). Further increasing B_{12} concentration in OP50 plates by 5-fold as well as addition of vitamin B_{12} to HB101 plates had no added protective effect (Figures 2E and S3A). Misfolded aggregation prone proteins underlie many neurodegenerative diseases. We found that B_{12} supplementation also had a protective effect in *C. elegans* models of amyotrophic lateral sclerosis (ALS) and Huntington's disease (Figure 2F), suggesting that B_{12} may protect against shared cellular defects resulting from proteotoxic stress.

We next sought to determine the impact of vitamin B_{12} on ATP availability, mitochondrial morphology, and ROS levels. Aβ animals fed B_{12} supplemented OP50 had significantly higher ATP levels compared to non-supplemented counterparts, while B_{12} had no effect on animals raised on HB101 (Figure 2G). Vitamin B_{12} supplementation did not alter mitochondrial gene transcription, protein levels, or respiration (Figures S2B–S2F) but did reduce mitochondrial fragmentation in Aβ animals fed OP50 without impacting mitochondria length in those raised on HB101 (Figure 2H). Severe B_{12} deficiency in *C. elegans* increases H_2O_2 content and decreases antioxidant defense (Bito et al., 2017). We found that addition of vitamin B_{12} to OP50 plates significantly reduced H_2O_2 and O_2^- in Aβ animals to levels observed in those raised on HB101 (Figures 2I and 2J). Together, these results show that vitamin B_{12} supplementation has a protective effect on Aβ animals fed the OP50 diet.

Vitamin B_{12} given during adulthood has protective effects

Subclinical B_{12} deficiency is common primarily in older individuals (Green et al., 2017). Thus, we sought to determine if manipulation

Version of record at: https://doi.org/10.1016/j.celrep.2021.109753

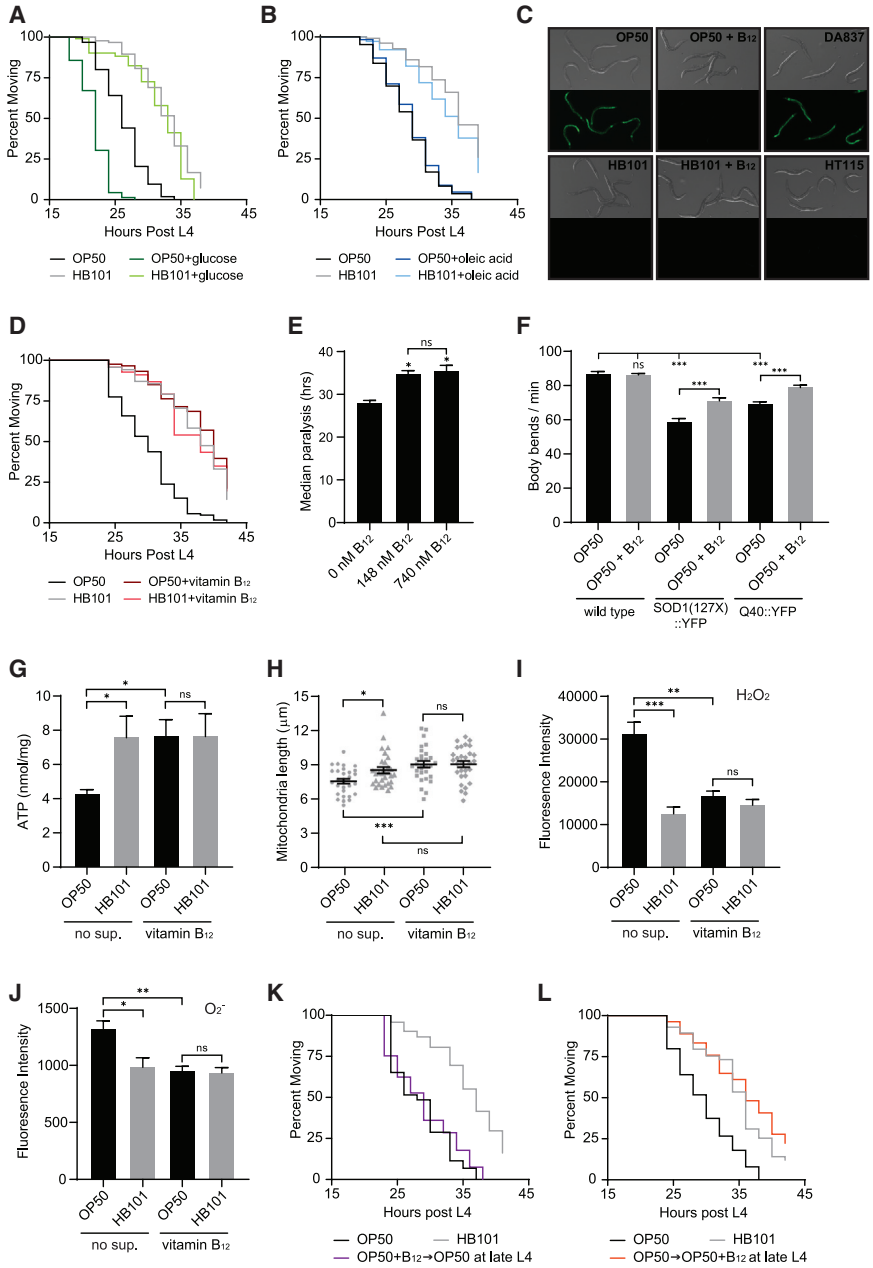

Figure 2. Vitamin B_{12} is the protective factor in the HB101 diet

(A) Supplementation with 10 mM glucose accelerated paralysis of Aβ animals fed OP50 but did not eliminate the dietary shift ($n \geq 102$).

(B) Supplementation with 0.3 mM oleic acid did not affect Aβ-induced paralysis ($n \geq 174$).

(C) *Pacdh-1*::GFP expression was induced in animals fed OP50 and DA837, but not OP50+B_{12}, HB101, HB101+B_{12}, and HT115.

(D) Supplementation with 148 nM vitamin B_{12} eliminated the impact of bacterial diet on paralysis of Aβ animals ($n \geq 139$).

(E) Supplementation with 740 nM B_{12} had no added protective effect compared to 148 nM B_{12} ($n = 3$); $^*p < 0.05$ compared to the no-supplementation control.

(F) B_{12} supplementation enhanced motility in *C. elegans* models of amyotrophic lateral sclerosis (ALS) and Huntington's disease but did not affect the WT ($n = 15$).

(G) Vitamin B_{12} increased ATP levels in Aβ animals fed OP50 compared to those without B_{12} supplementation (no sup.; $n = 6$).

(H) Vitamin B_{12} increased average mitochondrial length in Aβ animals fed OP50 ($n = 30$).

(I) Vitamin B_{12} reduced H_2O_2, measured with H_2DCFDA, in Aβ animals fed OP50 ($n = 9$).

(J) Vitamin B_{12} decreased O_2^-, measured with MitoSox, in Aβ animals fed OP50 ($n \geq 6$).

(K) Transfer of Aβ animals from OP50 plus vitamin B_{12} plates to B_{12}-free OP50 plates at the end of L4 eliminated the B_{12} protective effect ($n \geq 132$).

(L) Transfer of Aβ animals fed OP50 to OP50 plates supplemented with B_{12} at the end of L4 delayed paralysis ($n \geq 54$).

Error bars show SEM; $^*p < 0.05$, $^{**}p < 0.01$, and $^{***}p < 0.001$ one-way ANOVA with Dunnett's post-test. See also Figures S2 and S3.

of B_{12} availability during adulthood affected Aβ proteotoxicity in *C. elegans*. Animals grown on OP50 plates supplemented with vitamin B_{12} and then transferred to B_{12}-free OP50 plates at the end of the fourth larval stage (L4) exhibited Aβ-induced paralysis indistinguishable from animals raised on OP50 their entire life (Figures 2K and S3C). This demonstrates that a decrease in vitamin B_{12} during adulthood exacerbates Aβ proteotoxicity. Furthermore, Aβ animals first grown on OP50 and then transferred to OP50 plates supplemented with B_{12} at the end of L4 exhibited the same delay in paralysis as those fed a vitamin-B_{12}-rich diet their entire lifespan (Figures 2L and S3C). These results suggest potential benefit for dietary vitamin B_{12} supplementation later in life.

Protective effects of dietary B_{12} require methionine synthase

Vitamin B_{12} is an essential cofactor for methylmalonyl-coenzyme A (methylmalonyl-CoA) mutase (*C. elegans* MMCM-1), which converts methylmalonyl-CoA to succinyl-CoA in the propionyl-CoA breakdown pathway, and methionine synthase (*C. elegans* METR-1), which converts homocysteine (Hcy) to methionine in the methionine/SAMe cycle (Figure 3A). To define which pathway is required for the B_{12} protective effects, we determined the impact of mutations in *mmcm-1(ok1637)*; propionyl-CoA carboxylase *pcca-1(ok2282)*, which acts upstream of *mmcm-1*; and *metr-1(ok521)* on Aβ-induced paralysis. Loss of *pcca-1* and *mmcm-1* had no effect on the diet-induced shift in paralysis observed for Aβ animals grown on the different *E. coli* (Figures 3B, 3C, S4A, and S4B). However, the dietary shift was eliminated in *metr-1* mutants, which exhibited an even more severe phenotype than OP50-raised Aβ animals, which have only

Version of record at: https://doi.org/10.1016/j.celrep.2021.109753

CellPress
OPEN ACCESS

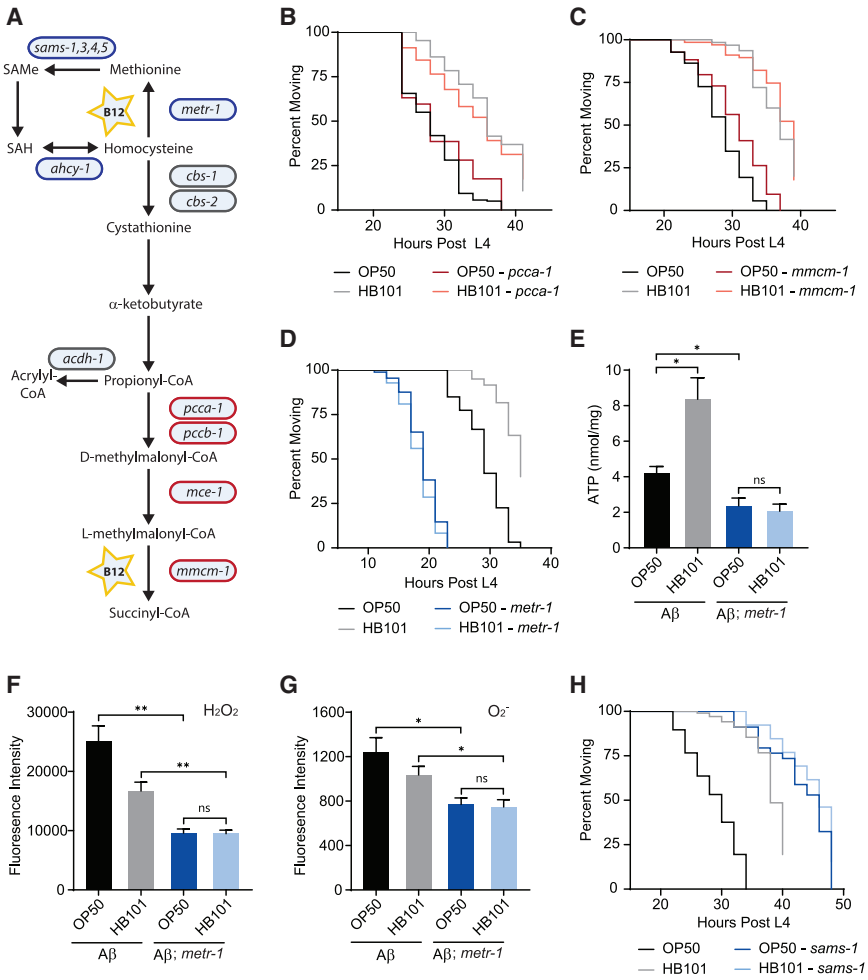

Figure 3. The methionine/SAMe cycle is required for the protective effects of vitamin B_{12}

(A) Diagram of vitamin-B_{12}-dependent pathways in *C. elegans*. Genes encoding enzymes that function in the methionine/SAMe cycle (blue) and the canonical B_{12} pathway (red) are indicated. SAMe, S-adenosylmethionine; SAH, s-adenosyl-l-homocysteine.

(B) *pcca-1(ok2282)* had no effect on the diet-induced shift in paralysis of Aβ animals ($n \geq 57$).

(C) Loss of *mmcm-1(ok1637)* did not eliminate the dietary shift ($n \geq 67$).

(D) *metr-1(ok521)* accelerated Aβ-induced paralysis and eliminated the impact of *E. coli* diet ($n \geq 60$).

(E) In *metr-1* mutant Aβ animals, ATP levels were low and unaffected by diet ($n \geq 7$).

(F) H_2O_2 levels were unaffected by diet in *metr-1* mutant Aβ animals ($n = 4$).

(G) O_2^- levels were unaffected by diet in *metr-1* mutant Aβ animals ($n \geq 6$).

(H) *sams-1(ok2946)* delayed Aβ-induced paralysis and eliminated the dietary shift ($n \geq 26$).

Error bars show SEM; $^*p < 0.05$ and $^{***}p < 0.001$, one-way ANOVA with Dunnett's post-test. See also Figure S4.

mild vitamin B_{12} deficiency (Figures 3D and S4C). Consistent with the behavioral data, loss of *metr-1* in Aβ animals reduced ATP levels and abolished the HB101 protective effect (Figure 3E). ROS content was also indistinguishable between *metr-1* Aβ animals raised on OP50 and HB101, though loss of *metr-1* caused an overall reduction in ROS levels (Figures 3F and 3G).

The methionine/SAMe cycle, transsulfuration pathway, folate cycle, and polyamine biosynthesis are all disrupted in the *metr-1* mutant. We found that loss of the SAMe synthetase SAMS-1, which catalyzes conversion of methionine to SAMe, eliminated the dietary shift and delayed Aβ-induced paralysis (Figures 3H and S4D). The opposite effect of the *metr-1* and *sams-1* mutations on time to paralysis is consistent with other previously observed phenotypes (Cabreiro et al., 2013). The elimination of dietary impact on Aβ-induced paralysis in both mutants suggests that the methionine/SAMe pathway is required for vitamin B_{12} protection.

Methionine and choline supplementation is protective in B_{12}-deficient Aβ animals

B_{12} deficiency reduces methionine synthase activity and can lead to Hcy accumulation (Figure 4A; Andra et al., 2021). We found that Aβ animals grown on OP50 had significantly increased Hcy, which was reduced by B_{12} supplementation (Figure 4B). Hyperhomocysteinemia is a modifiable risk factor for AD and results in oxidative stress (Bito et al., 2017; Smith and Refsum, 2016); thus, we sought to determine the effect of Hcy on Aβ-induced paralysis. Hcy supplementation accelerated paralysis of Aβ animals raised on OP50 and HB101 but did not change the dietary shift (Figures 4C and S4E). This suggests that the increased Hcy in animals fed OP50 did not underlie the effect of low dietary vitamin B_{12}. We next considered whether methionine level could impact Aβ toxicity. Methionine supplementation eliminated the dietary shift in paralysis (Figure 4D), having a beneficial effect on Aβ animals fed OP50 and a detrimental impact on those grown on HB101 (Figures 4D, S4F, and S4G). To establish if methionine acts directly in *C. elegans* or indirectly by altering bacterial metabolism, we determined if methionine supplementation could rescue the *metr-1* mutant, which is completely dependent on exogenous methionine (Hannich et al., 2009). Addition of methionine significantly delayed Aβ-induced paralysis and increased ATP in the *metr-1* mutant to the level observed in Aβ animals raised on OP50 (Figures 4E–4G). Bacterial diet did not affect the paralysis of Aβ-expressing *metr-1* mutants grown on plates supplemented with methionine (Figure 4F). Together, these results suggest that the impact of methionine supplementation is not due to a change in bacterial metabolism.

The loss of the dietary shift in Aβ-induced paralysis in the *sams-1* mutant (Figure 3H) suggested that the methionine/SAMe cycle is required for the protective effects of B_{12}. SAMe, the main

Version of record at: https://doi.org/10.1016/j.celrep.2021.109753

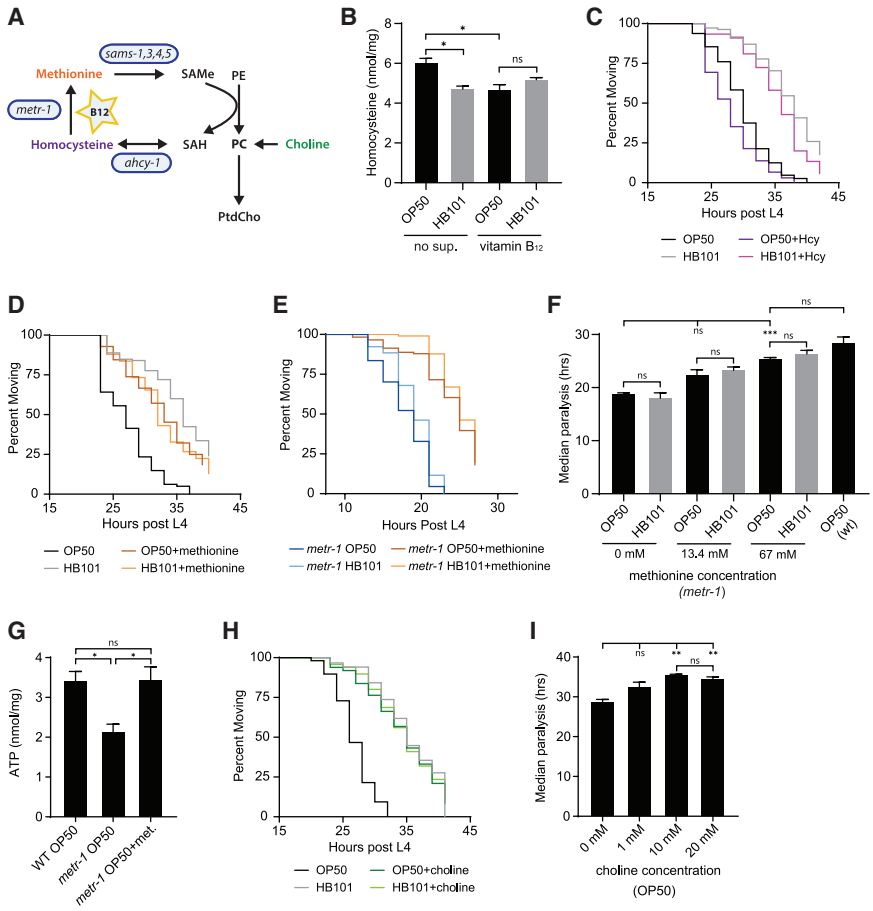

Figure 4. Methionine and choline supplementation reduce Aβ proteotoxic effects in B_{12}-deficient animals

(A) Schematic diagram shows link between the vitamin-B_{12}-dependent methionine/SAMe cycle (blue) and phospholipid biosynthesis. SAH, s-adenosyl-l-homocysteine; PE, phosphoethanolamine; PC, phosphocholine; PtdCho, phosphatidylcholine. PtdCho can be synthesized from choline or methylation of PE.

(B) Aβ animals grown on OP50 had higher levels of Hcy compared to those raised on HB101- or B_{12}-supplemented plates (n = 4).

(C) Supplementation with 15 mM Hcy accelerated paralysis of Aβ animals grown on both OP50 and HB101 but did not eliminate the dietary shift ($n \geq 105$).

(D) Supplementation with 13.4 mM L-methionine eliminated the diet-induced shift in paralysis ($n \geq 116$).

(E) Methionine supplementation (67 mM) delayed Aβ-induced paralysis in the *metr-1* mutant ($n \geq 67$).

(F) Supplementation of the *metr-1* mutant with 13.4 mM and 67 mM methionine delayed the median time to Aβ-induced paralysis ($n \geq 3$).

(G) Supplementation with 67 mM methionine caused a significant increase in ATP in the *metr-1* mutant ($n \geq 4$).

(H) Supplementation with 10 mM choline eliminated the impact of bacterial diet on Aβ-induced paralysis ($n \geq 107$).

(I) Choline concentration above 10 mM had no additional protective effect ($n \geq 3$).

Error bars show SEM; $^{*}p < 0.05$, $^{**}p < 0.01$, and $^{***}p < 0.001$, one-way ANOVA with Dunnett's post-test. See also Figure S4.

methyl donor in cells, is utilized by many methyltransferases, which transfer methyl groups to nucleic acids, histones, and phospholipids. Since addition and removal of vitamin B_{12} beginning at adulthood has beneficial and detrimental effects, respectively (Figures 2K and 2L), we reasoned that it was unlikely that SAMe impacted paralysis by having an effect on DNA and protein methylation that regulates transcription. Phosphatidylcholine (PtdCho), a major component of membranes, can be synthesized by SAMe-dependent methylation of phosphoethanolamine or directly from choline through the Kennedy pathway (Figure 4A; Brendza et al., 2007; Palavalli et al., 2006), and reduced PtdCho has been observed in individuals with AD (Whiley et al., 2014). Supplementation of OP50 plates with choline delayed Aβ-induced paralysis, eliminating the dietary shift (Figure 4H). Choline provided no protection for Aβ animals fed HB101, and further increasing choline concentration did not have additional benefit for those fed OP50 (Figures 4H and 4I). These data are consistent with a model in which vitamin-B_{12}-dependent methionine/SAMe cycle activity increases PtdCho production to reduce Aβ proteotoxic effects.

DISCUSSION

Diet is a modifiable risk factor for AD; however, the impact of specific nutrients on disease onset and progression is difficult to define due to human genetic diversity and diet complexity. Here, we used the genetically tractable nematode *C. elegans*, which consumes a simple *E. coli* diet, and discovered that vitamin B_{12} reduces Aβ proteotoxicity. In Aβ-expressing animals, vitamin B_{12} increased ATP levels, reduced mitochondrial fragmentation, and decreased ROS but did not impact Aβ levels. Currently, there is no effective disease-modifying treatment for AD, and therapeutics designed to reduce Aβ levels have failed (Long and Holtzman, 2019). Our results suggest that vitamin B_{12} supplementation could be a therapeutic approach to target energy crisis and oxidative stress, pathogenic features of AD triggered by Aβ accumulation.

Subclinical B_{12} deficiency is common, with a prevalence of 10%–15% among individuals older than 60 years and up to 35% among those older than 80 years (Green et al., 2017), and low B_{12} status may be a modifiable risk factor for AD (Vogiatzoglou et al., 2008). Meta-analyses of clinical trials have suggested that administration of B vitamins does not prevent cognitive decline (Clarke et al., 2014; Ford and Almeida, 2019). However, most participants did not exhibit preexisting cognitive defects, trial durations were insufficient to observe cognitive decline, and prior B_{12} status was not considered. Our results show that vitamin B_{12} supplementation was beneficial for Aβ-expressing *C. elegans* with mild B_{12} deficiency but did not offer additional protection for non-deficient animals. Consistent with our work,

studies focused on individuals with low dietary vitamin B showed that supplementation with B vitamins preserved cognition (Kang et al., 2008) and slowed brain atrophy (Smith et al., 2010). Thus, the therapeutic potential for vitamin B_{12} is likely dependent on preexisting B_{12} status. How genetic profile and other components of the complex human diet further impact probability of vitamin B_{12} therapeutic success will need to be resolved.

Reduced ATP level hinders cellular ability to maintain ionic gradients, leading to increased intracellular Ca^{2+}, synaptic dysfunction, and neuronal death, as observed in AD pathogenesis. Mild vitamin B_{12} deficiency led to reduced ATP in Aβ-expressing, but not wild-type, *C. elegans*, suggesting that low B_{12} status is detrimental during proteotoxic stress. Despite decreasing mitochondrial fragmentation, we found vitamin B_{12} did not prevent Aβ-induced defects in cellular respiration. Rather, B_{12} status appears to have an impact on the Aβ-induced energy crisis that precedes mitochondrial dysfunction (Fong et al., 2016). Both Aβ oligomers and oxidative stress can induce membrane damage, which leads to ion leakage and necessitates increased ATP expenditure by ATPases to maintain ionic gradients and membrane potential (Butterfield and Halliwell, 2019; Ronquist and Waldenström, 2003; Yang et al., 2017). Glycolysis is the dominant ATP production pathway used to fuel plasma membrane ATPases (Ronquist and Waldenström, 2003; Yellen, 2018), and studies suggest a link between impaired glucose metabolism and the severity of neurodegenerative diseases (An et al., 2018; Zhang et al., 2021). We found that dietary vitamin B_{12} reduced energy crisis and was protective in *C. elegans* models of AD, Huntington's disease, and ALS.

Vitamin B_{12} causes resistance to pathogen stress in *C. elegans*, and this requires the methylmalonyl-CoA mutase MMCM-1 (Revtovich et al., 2019). In contrast, our work showed that loss of *metr-1* or *sams-1* eliminated the effect of diet on Aβ-induced paralysis, suggesting that B_{12} defends against proteotoxic stress by acting as a cofactor for methionine synthase, impacting the methionine/SAMe cycle. While methionine restriction results in epigenetic changes that extend lifespan in many organisms, including *C. elegans* (Grandison et al., 2009; Orentreich et al., 1993; Parkhitko et al., 2019), our work suggests that a reduction in methionine synthase activity is detrimental for nematodes under proteotoxic stress. Reduced methionine lowers SAMe, which is required for methylation-dependent synthesis of PtdCho. Altered ratios of phospholipids can influence energy metabolism as well as ion leak across the plasma membrane (Ronquist and Waldenström, 2003; van der Veen et al., 2017), and reduced PtdCho has been observed in individuals with AD (Whiley et al., 2014). Here, we found that choline supplementation, which increases PtdCho synthesis via the Kennedy pathway (Walker et al., 2011), eliminated the effect of vitamin B_{12} on paralysis of Aβ animals. Together, our results support a model in which vitamin B_{12} status impacts methionine/SAMe-cycle-dependent phospholipid homeostasis to protect against Aβ-induced proteotoxicity.

STAR★METHODS

Detailed methods are provided in the online version of this paper and include the following:

SUPPLEMENTAL INFORMATION

Supplemental information can be found online at https://doi.org/10.1016/j.celrep.2021.109753.

ACKNOWLEDGMENTS

We thank Jeffrey Caplan from the University of Delaware BioImaging Center for writing the script to measure mitochondrial length. Nematode strains were provided by the *Caenorhabditis* Genetics Center, which is supported by the NIH-ORIP (P40 OD010440). Microscopy access was supported by grants from the NIH-NIGMS (P20 GM103446), NSF (IIA-1301765), and the State of Delaware. This work was supported by a University of Delaware Graduate Scholars award (to A.B.L.), NIH-NIGMS INBRE Pilot Project grant P20 GM103446, NIGMS-NIH Alzheimer's Supplement P20 GM103446-21S1, and University of Delaware Research Foundation Award 18A00929 (to J.E.T.).

AUTHOR CONTRIBUTIONS

Conceptualization, A.B.L., K.K., and J.E.T.; investigation, A.B.L., K.K., and J.E.T.; writing – original draft, A.B.L. and J.E.T.; writing – review & editing, A.B.L., K.K., and J.E.T.; visualization, A.B.L. and J.E.T.; supervision, J.E.T.; funding acquisition, J.E.T.

DECLARATION OF INTERESTS

The authors declare no competing interests.

Received: February 24, 2021
Revised: August 5, 2021
Accepted: September 1, 2021
Published: September 28, 2021

REFERENCES

Alcántar-Fernández, J., Navarro, R.E., Salazar-Martínez, A.M., Pérez-Andrade, M.E., and Miranda-Ríos, J. (2018). Caenorhabditis elegans respond to high-glucose diets through a network of stress-responsive transcription factors. PLoS ONE *13*, e0199888.

An, Y., Varma, V.R., Varma, S., Casanova, R., Dammer, E., Pletnikova, O., Chia, C.W., Egan, J.M., Ferrucci, L., Troncoso, J., et al. (2018). Evidence for brain glucose dysregulation in Alzheimer's disease. Alzheimers Dement. *14*, 318–329.

Andra, A., Tanigawa, S., Bito, T., Ishihara, A., Watanabe, F., and Yabuta, Y. (2021). Effects of Vitamin B_{12} Deficiency on Amyloid-β Toxicity in *Caenorhabditis elegans*. Antioxidants *10*, 962.

Baker, B.M., Nargund, A.M., Sun, T., and Haynes, C.M. (2012). Protective coupling of mitochondrial function and protein synthesis via the eIF2α kinase GCN-2. PLoS Genet. *8*, e1002760.

Bito, T., Misaki, T., Yabuta, Y., Ishikawa, T., Kawano, T., and Watanabe, F. (2017). Vitamin B_{12} deficiency results in severe oxidative stress, leading to memory retention impairment in Caenorhabditis elegans. Redox Biol. *11*, 21–29.

Brendza, K.M., Haakenson, W., Cahoon, R.E., Hicks, L.M., Palavalli, L.H., Chiapelli, B.J., McLaird, M., McCarter, J.P., Williams, D.J., Hresko, M.C., and Jez, J.M. (2007). Phosphoethanolamine N-methyltransferase (PMT-1) catalyses the first reaction of a new pathway for phosphocholine biosynthesis in Caenorhabditis elegans. Biochem. J. *404*, 439–448.

Brenner, S. (1974). The genetics of Caenorhabditis elegans. Genetics *77*, 71–94.

Brooks, K.K., Liang, B., and Watts, J.L. (2009). The influence of bacterial diet on fat storage in C. elegans. PLoS ONE *4*, e7545.

Butterfield, D.A., and Halliwell, B. (2019). Oxidative stress, dysfunctional glucose metabolism and Alzheimer disease. Nat. Rev. Neurosci. *20*, 148–160.

Cabreiro, F., Au, C., Leung, K.Y., Vergara-Irigaray, N., Cochemé, H.M., Noori, T., Weinkove, D., Schuster, E., Greene, N.D.E., and Gems, D. (2013). Metformin retards aging in C. elegans by altering microbial folate and methionine metabolism. Cell *153*, 228–239.

Cacho-Valadez, B., Muñoz-Lobato, F., Pedrajas, J.R., Cabello, J., Fierro-González, J.C., Navas, P., Swoboda, P., Link, C.D., and Miranda-Vizuete, A. (2012). The characterization of the *Caenorhabditis elegans* mitochondrial thioredoxin system uncovers an unexpected protective role of thioredoxin reductase 2 in β-amyloid peptide toxicity. Antioxid. Redox Signal. *16*, 1384–1400.

Chakravorty, A., Jetto, C.T., and Manjithaya, R. (2019). Dysfunctional Mitochondria and Mitophagy as Drivers of Alzheimer's Disease Pathogenesis. Front. Aging Neurosci. *11*, 311.

Chartier-Harlin, M.C., Crawford, F., Houlden, H., Warren, A., Hughes, D., Fidani, L., Goate, A., Rossor, M., Roques, P., Hardy, J., et al. (1991). Early-onset Alzheimer's disease caused by mutations at codon 717 of the β-amyloid precursor protein gene. Nature *353*, 844–846.

Chaya, T., Patel, S., Smith, E.M., Lam, A., Miller, E., Clupper, M., Kervin, K., and Tanis, J.E. (2021). A C. elegans genome-wide RNAi screen for altered levamisole sensitivity identifies genes required for muscle function. G3 (Bethesda) *11*, jkab047.

Chen, G.F., Xu, T.H., Yan, Y., Zhou, Y.R., Jiang, Y., Melcher, K., and Xu, H.E. (2017). Amyloid beta: structure, biology and structure-based therapeutic development. Acta Pharmacol. Sin. *38*, 1205–1235.

Clarke, R., Bennett, D., Parish, S., Lewington, S., Skeaff, M., Eussen, S.J.P.M., Lewerin, C., Stott, D.J., Armitage, J., Hankey, G.J., et al.; B-Vitamin Treatment Trialists' Collaboration (2014). Effects of homocysteine lowering with B vitamins on cognitive aging: meta-analysis of 11 trials with cognitive data on 22,000 individuals. Am. J. Clin. Nutr. *100*, 657–666.

Cline, E.N., Bicca, M.A., Viola, K.L., and Klein, W.L. (2018). The Amyloid-β Oligomer Hypothesis: Beginning of the Third Decade. J. Alzheimers Dis. *64* (*s1*), S567–S610.

Cogliati, S., Clementi, V., Francisco, M., Crespo, C., Argañaraz, F., and Grau, R. (2020). Bacillus Subtilis Delays Neurodegeneration and Behavioral Impairment in the Alzheimer's Disease Model Caenorhabditis Elegans. J. Alzheimers Dis. *73*, 1035–1052.

De Strooper, B., and Karran, E. (2016). The Cellular Phase of Alzheimer's Disease. Cell *164*, 603–615.

Deline, M.L., Vrablik, T.L., and Watts, J.L. (2013). Dietary supplementation of polyunsaturated fatty acids in Caenorhabditis elegans. J. Vis. Exp. *81*, 50879.

Drake, J., Link, C.D., and Butterfield, D.A. (2003). Oxidative stress precedes fibrillar deposition of Alzheimer's disease amyloid β-peptide (1-42) in a transgenic Caenorhabditis elegans model. Neurobiol. Aging *24*, 415–420.

Fang, E.F., Hou, Y., Palikaras, K., Adriaanse, B.A., Kerr, J.S., Yang, B., Lautrup, S., Hasan-Olive, M.M., Caponio, D., Dan, X., et al. (2019). Mitophagy inhibits amyloid-β and tau pathology and reverses cognitive deficits in models of Alzheimer's disease. Nat. Neurosci. *22*, 401–412.

Fong, S., Teo, E., Ng, L.F., Chen, C.B., Lakshmanan, L.N., Tsoi, S.Y., Moore, P.K., Inoue, T., Halliwell, B., and Gruber, J. (2016). Energy crisis precedes global metabolic failure in a novel Caenorhabditis elegans Alzheimer Disease model. Sci. Rep. *6*, 33781.

Fonte, V., Dostal, V., Roberts, C.M., Gonzales, P., Lacor, P.N., Velasco, P.T., Magrane, J., Dingwell, N., Fan, E.Y., Silverman, M.A., et al. (2011). A glycine zipper motif mediates the formation of toxic β-amyloid oligomers in vitro and in vivo. Mol. Neurodegener. *6*, 61.

Ford, A.H., and Almeida, O.P. (2019). Effect of Vitamin B Supplementation on Cognitive Function in the Elderly: A Systematic Review and Meta-Analysis. Drugs Aging *36*, 419–434.

Goate, A., Chartier-Harlin, M.C., Mullan, M., Brown, J., Crawford, F., Fidani, L., Giuffra, L., Haynes, A., Irving, N., James, L., et al. (1991). Segregation of a missense mutation in the amyloid precursor protein gene with familial Alzheimer's disease. Nature *349*, 704–706.

Grandison, R.C., Piper, M.D.W., and Partridge, L. (2009). Amino-acid imbalance explains extension of lifespan by dietary restriction in Drosophila. Nature *462*, 1061–1064.

Green, R., Allen, L.H., Bjørke-Monsen, A.L., Brito, A., Guéant, J.L., Miller, J.W., Molloy, A.M., Nexo, E., Stabler, S., Toh, B.H., et al. (2017). Vitamin B_{12} deficiency. Nat. Rev. Dis. Primers *3*, 17040.

Han, B., Sivaramakrishnan, P., Lin, C.J., Neve, I.A.A., He, J., Tay, L.W.R., Sowa, J.N., Sizovs, A., Du, G., Wang, J., et al. (2017). Microbial Genetic Composition Tunes Host Longevity. Cell *169*, 1249–1262.e13.

Hannich, J.T., Entchev, E.V., Mende, F., Boytchev, H., Martin, R., Zagoriy, V., Theumer, G., Riezman, I., Riezman, H., Knölker, H.J., and Kurzchalia, T.V. (2009). Methylation of the sterol nucleus by STRM-1 regulates dauer larva formation in Caenorhabditis elegans. Dev. Cell *16*, 833–843.

Hassan, W.M., Dostal, V., Huemann, B.N., Yerg, J.E., and Link, C.D. (2015). Identifying Aβ-specific pathogenic mechanisms using a nematode model of Alzheimer's disease. Neurobiol. Aging *36*, 857–866.

Kang, J.H., Cook, N., Manson, J., Buring, J.E., Albert, C.M., and Grodstein, F. (2008). A trial of B vitamins and cognitive function among women at high risk of cardiovascular disease. Am. J. Clin. Nutr. *88*, 1602–1610.

Koopman, M., Michels, H., Dancy, B.M., Kamble, R., Mouchiroud, L., Auwerx, J., Nollen, E.A.A., and Houtkooper, R.H. (2016). A screening-based platform for the assessment of cellular respiration in Caenorhabditis elegans. Nat. Protoc. *11*, 1798–1816.

Lee, S.J., Murphy, C.T., and Kenyon, C. (2009). Glucose shortens the life span of C. elegans by downregulating DAF-16/FOXO activity and aquaporin gene expression. Cell Metab. *10*, 379–391.

Lin, M.T., and Beal, M.F. (2006). Mitochondrial dysfunction and oxidative stress in neurodegenerative diseases. Nature *443*, 787–795.

Link, C.D. (1995). Expression of human β-amyloid peptide in transgenic Caenorhabditis elegans. Proc. Natl. Acad. Sci. USA *92*, 9368–9372.

Long, J.M., and Holtzman, D.M. (2019). Alzheimer Disease: An Update on Pathobiology and Treatment Strategies. Cell *179*, 312–339.

Lublin, A.L., and Link, C.D. (2013). Alzheimer's disease drug discovery: in vivo screening using Caenorhabditis elegans as a model for β-amyloid peptide-induced toxicity. Drug Discov. Today. Technol. *10*, e115–e119.

MacNeil, L.T., Watson, E., Arda, H.E., Zhu, L.J., and Walhout, A.J.M. (2013). Diet-induced developmental acceleration independent of TOR and insulin in C. elegans. Cell *153*, 240–252.

McColl, G., Roberts, B.R., Pukala, T.L., Kenche, V.B., Roberts, C.M., Link, C.D., Ryan, T.M., Masters, C.L., Barnham, K.J., Bush, A.I., and Cherny, R.A. (2012). Utility of an improved model of amyloid-beta ($A\beta_{1-42}$) toxicity in Caenorhabditis elegans for drug screening for Alzheimer's disease. Mol. Neurodegener. *7*, 57.

Neve, I.A.A., Sowa, J.N., Lin, C.J., Sivaramakrishnan, P., Herman, C., Ye, Y., Han, L., and Wang, M.C. (2020). Escherichia coli metabolite profiling leads to the development of an RNA interference strain for Caenorhabditis elegans. G3 (Bethesda) *10*, 189–198.

Ng, L.F., and Gruber, J. (2019). Measurement of Respiration Rate in Live *Caenorhabditis elegans*. Bio Protoc. *9*, e3243.

Orentreich, N., Matias, J.R., DeFelice, A., and Zimmerman, J.A. (1993). Low methionine ingestion by rats extends life span. J. Nutr. *123*, 269–274.

Pagani, L., and Eckert, A. (2011). Amyloid-Beta interaction with mitochondria. Int. J. Alzheimers Dis. *2011*, 925050.

Palavalli, L.H., Brendza, K.M., Haakenson, W., Cahoon, R.E., McLaird, M., Hicks, L.M., McCarter, J.P., Williams, D.J., Hresko, M.C., and Jez, J.M. (2006). Defining the role of phosphomethylethanolamine N-methyltransferase from Caenorhabditis elegans in phosphocholine biosynthesis by biochemical and kinetic analysis. Biochemistry *45*, 6056–6065.

Parkhitko, A.A., Jouandin, P., Mohr, S.E., and Perrimon, N. (2019). Methionine metabolism and methyltransferases in the regulation of aging and lifespan extension across species. Aging Cell *18*, e13034.

Revtovich, A.V., Lee, R., and Kirienko, N.V. (2019). Interplay between mitochondria and diet mediates pathogen and stress resistance in Caenorhabditis elegans. PLoS Genet. *15*, e1008011.

Ronquist, G., and Waldenström, A. (2003). Imbalance of plasma membrane ion leak and pump relationship as a new aetiological basis of certain disease states. J. Intern. Med. *254*, 517–526.

Rousakis, A., Vlassis, A., Vlanti, A., Patera, S., Thireos, G., and Syntichaki, P. (2013). The general control nonderepressible-2 kinase mediates stress response and longevity induced by target of rapamycin inactivation in Caenorhabditis elegans. Aging Cell *12*, 742–751.

Schulz, T.J., Zarse, K., Voigt, A., Urban, N., Birringer, M., and Ristow, M. (2007). Glucose restriction extends Caenorhabditis elegans life span by inducing mitochondrial respiration and increasing oxidative stress. Cell Metab. *6*, 280–293.

Shen, X., Ellis, R.E., Sakaki, K., and Kaufman, R.J. (2005). Genetic interactions due to constitutive and inducible gene regulation mediated by the unfolded protein response in C. elegans. PLoS Genet. *1*, e37.

Shtonda, B.B., and Avery, L. (2006). Dietary choice behavior in Caenorhabditis elegans. J. Exp. Biol. *209*, 89–102.

Smith, A.D., and Refsum, H. (2016). Homocysteine, B Vitamins, and Cognitive Impairment. Annu. Rev. Nutr. *36*, 211–239.

Smith, A.D., Smith, S.M., de Jager, C.A., Whitbread, P., Johnston, C., Agacinski, G., Oulhaj, A., Bradley, K.M., Jacoby, R., and Refsum, H. (2010). Homocysteine-lowering by B vitamins slows the rate of accelerated brain atrophy in mild cognitive impairment: a randomized controlled trial. PLoS ONE *5*, e12244.

Sorrentino, V., Romani, M., Mouchiroud, L., Beck, J.S., Zhang, H., D'Amico, D., Moullan, N., Potenza, F., Schmid, A.W., Rietsch, S., et al. (2017). Enhancing mitochondrial proteostasis reduces amyloid-β proteotoxicity. Nature *552*, 187–193.

Steinkraus, K.A., Smith, E.D., Davis, C., Carr, D., Pendergrass, W.R., Sutphin, G.L., Kennedy, B.K., and Kaeberlein, M. (2008). Dietary restriction suppresses proteotoxicity and enhances longevity by an hsf-1-dependent mechanism in Caenorhabditis elegans. Aging Cell *7*, 394–404.

Teo, E., Ravi, S., Barardo, D., Kim, H.S., Fong, S., Cazenave-Gassiot, A., Tan, T.Y., Ching, J., Kovalik, J.P., Wenk, M.R., et al. (2019). Metabolic stress is a primary pathogenic event in transgenic *Caenorhabditis elegans* expressing pan-neuronal human amyloid beta. eLife *8*, e50069.

Thelen, M., and Brown-Borg, H.M. (2020). Does Diet Have a Role in the Treatment of Alzheimer's Disease? Front. Aging Neurosci. *12*, 617071.

Touroutine, D., and Tanis, J.E. (2020). A Rapid, SuperSelective Method for Detection of Single Nucleotide Variants in *Caenorhabditis elegans*. Genetics *216*, 343–352.

van der Veen, J.N., Kennelly, J.P., Wan, S., Vance, J.E., Vance, D.E., and Jacobs, R.L. (2017). The critical role of phosphatidylcholine and phosphatidylethanolamine metabolism in health and disease. Biochim. Biophys. Acta Biomembr. *1859* (*9 Pt B*), 1558–1572.

Virk, B., Correia, G., Dixon, D.P., Feyst, I., Jia, J., Oberleitner, N., Briggs, Z., Hodge, E., Edwards, R., Ward, J., et al. (2012). Excessive folate synthesis limits lifespan in the C. elegans: E. coli aging model. BMC Biol. *10*, 67.

Virk, B., Jia, J., Maynard, C.A., Raimundo, A., Lefebvre, J., Richards, S.A., Chetina, N., Liang, Y., Helliwell, N., Cipinska, M., and Weinkove, D. (2016). Folate Acts in E. coli to Accelerate C. elegans Aging Independently of Bacterial Biosynthesis. Cell Rep. *14*, 1611–1620.

Vogiatzoglou, A., Refsum, H., Johnston, C., Smith, S.M., Bradley, K.M., de Jager, C., Budge, M.M., and Smith, A.D. (2008). Vitamin B12 status and rate of brain volume loss in community-dwelling elderly. Neurology *71*, 826–832.

Walker, A.K., Jacobs, R.L., Watts, J.L., Rottiers, V., Jiang, K., Finnegan, D.M., Shioda, T., Hansen, M., Yang, F., Niebergall, L.J., et al. (2011). A conserved SREBP-1/phosphatidylcholine feedback circuit regulates lipogenesis in metazoans. Cell *147*, 840–852.

Wang, X., Wang, W., Li, L., Perry, G., Lee, H., and Zhu, X. (2014). Oxidative stress and mitochondrial dysfunction in Alzheimer's disease. Biochim. Biophys. Acta Mol. Basis Dis. *1842*, 1240–1247.

Watson, E., MacNeil, L.T., Ritter, A.D., Yilmaz, L.S., Rosebrock, A.P., Caudy, A.A., and Walhout, A.J.M. (2014). Interspecies systems biology uncovers metabolites affecting C. elegans gene expression and life history traits. Cell *156*, 759–770.

Watson, E., Olin-Sandoval, V., Hoy, M.J., Li, C.H., Louisse, T., Yao, V., Mori, A., Holdorf, A.D., Troyanskaya, O.G., Ralser, M., and Walhout, A.J. (2016). Metabolic network rewiring of propionate flux compensates vitamin B12 deficiency in C. elegans. eLife *5*, e17670.

Wei, W., and Ruvkun, G. (2020). Lysosomal activity regulates *Caenorhabditis elegans* mitochondrial dynamics through vitamin B12 metabolism. Proc. Natl. Acad. Sci. USA *117*, 19970–19981.

Whiley, L., Sen, A., Heaton, J., Proitsi, P., García-Gómez, D., Leung, R., Smith, N., Thambisetty, M., Kloszewska, I., Mecocci, P., et al.; AddNeuroMed Consortium (2014). Evidence of altered phosphatidylcholine metabolism in Alzheimer's disease. Neurobiol. Aging *35*, 271–278.

Yang, T., Li, S., Xu, X.H., Walsh, D.M., and Selkoe, D.J. (2017). Large Soluble Oligomers of Amyloid beta from Alzheimer Brain Are Far Less Neuroactive Than the Smaller Oligomers to Which They Dissociate. J. Neurosci. *37*, 152–163.

Yellen, G. (2018). Fueling thought: Management of glycolysis and oxidative phosphorylation in neuronal metabolism. J. Cell Biol. *217*, 2235–2246.

Yoon, D.S., Lee, M.-H., and Cha, D.S. (2018). Measurement of Intracellular ROS in *Caenorhabditis elegans* Using 2′,7′-Dichlorodihydrofluorescein Diacetate. Bio Protoc. *8*, e2774.

Zhang, X., Alshakhshir, N., Zhao, L., Wood, L., and Kaplin, A.I. (2021). Glycolytic Metabolism, Brain Resilience, and Alzheimer's Disease. Front. Neurosci. *15*, 662242.

Version of record at: https://doi.org/10.1016/j.celrep.2021.109753

STAR★METHODS

KEY RESOURCES TABLE

REAGENT or RESOURCE	SOURCE	IDENTIFIER
Antibodies		
anti-β-Amyloid 6E10	BioLegend	Cat#803001; RRID: AB_2564653
anti-α-tubulin A11	Millipore Sigma	Cat#T9026; RRID: AB_477593
Anti-NDUFS3	Abcam	Cat#ab14711; RRID: AB_301429
Goat anti-Mouse IgG (H+L) Secondary Antibody, HRP	ThermoFisher Scientific	Cat#31430; RRID: AB_228307
Bacterial and virus strains		
Escherichia coli OP50	*Caenorhabditis* Genetics Center (CGC)	N/A
Escherichia coli HB101	CGC	N/A
Escherichia coli HT115	CGC	N/A
Escherichia coli DA837	CGC	N/A
Chemicals, peptides, and recombinant proteins		
D(+)-glucose	Fisher Scientific	Cat#: AC410955000 CAS: 50-99-7
Sodium Homogamma Linolenate	Nu-Chek Prep	Cat#: S-1143, CAS: 65881-87-0
Oleic Acid	ThermoFisher Scientific	Cat#:31997, CAS: 112-80-1
Methylcobalamin	Millipore Sigma	Cat#: M9756, CAS: 13422-55-4
L-methionine	Fisher Scientific	Cat#: AC166160025 CAS: 63-68-3
DL-Homocysteine	Millipore Sigma	Cat#: H4628, CAS: 454-29-5
Choline Chloride	Millipore Sigma	Cat#: C7017-5G, CAS:67-48-1
Levamisole hydrochloride	Fisher Scientific	Cat#: AC187870100 CAS: 16595-80-5
EDTA-free Protease Inhibitor cocktail	Roche	Cat#: 4693159001
NP-40	ThermoFisher Scientific	Cat#: 85124, CAS: 9016-45-9
Sodium Dodecyl Sulfate	Fisher Bioreagents	Cat#: BP1311-200, CAS: 151-21-3,7732-18-5
Sodium Chloride (NaCl)	Fisher Bioreagents	Cat#: BP358-1 CAS:7647-14-5
1M Tris-HCl pH 8.3	Teknova	Cat#: T5083
Tris Base	Fisher Bioreagents	Cat#: BP152-500, CAS: 77-86-1
TRIS-buffered saline (TBS, 10x)	Alfa Aesar	Cat#: J62938-K2, CAS: 77-86-1
Tween-20	Fisher Bioreagents	Cat#: BP337-100 CAS: 9005-64-5
Non-Fat Powdered Milk	Boston BioProducts	Cat#: P-1400
β-meracaptoethanol	Fisher Scientific	Cat#: AC125470100 CAS: 60-24-2
Bromophenol Blue	Fisher Scientific	Cat#: AC403140050 CAS: 115-39-9
Urea	ThermoFisher Scientific	Cat#: 29700, CAS: 57-13-6
Glycerol	Fisher Bioreagents	Cat#: BP229-1, CAS: 56-81-5
10x Tris/Glycine/SDS Buffer	BioRad	Cat#: 1210732
Glycine	Fisher Bioreagents	Cat#: BP381-500 CAS:56-40-6
Methanol	Fisher Chemical	Cat#: A454-4, CAS: 67-56-1
16.5% Mini-Protean Tris-Tricine Gel	BioRad	Cat#: 4563063
10% Mini-Protean TGX Precast Protein Gels	BioRad	Cat#: 4561033
Trizol	ThermoFisher Scientific	Cat#: 15596018
Chloroform	Crescent Chemical Co.	Cat#: 39553.01, CAS: 67-66-3
RNase-Free DNase Set	QIAGEN	Cat#: 79254
PowerUp SYBR Green Master Mix	Applied Biosystems	Cat#: A25741

(*Continued on next page*)

Continued

REAGENT or RESOURCE	SOURCE	IDENTIFIER
0.5M EDTA pH 8.0	Invitrogen	Cat#: 15575-038
2′7′-Dichlorofluorescin diacetate	Millipore Sigma	Cat#: D6883-250, CAS: 4091-99-0
Nile Red	ThermoFisher Scientific	Cat#: N1142
Agarose	Fisher Bioreagents	Cat#:BP160-500, CAS: 9012-36-6
Carbonyl cyanide-p-trifluoromethoxyphenylhydrazone (FCCP)	Millipore Sigma	Cat#: C2920-10, CAS: 370-86-5
DMSO (Dimethyl Sulfoxide) LC-MS Grade	ThermoFisher Scientific	Cat#: 85190, Cas:67-68-5
Sodium Azide	Acros Organics	Cat#: 19038-1000, CAS: 26629-22-8
Paraformaldehyde (16%) Solution EM Grade	Electron Microscopy Sciences	Cat#: 15710, CAS: 30525-89-4
Water, Molecular Grade, Sterile, DEPC Free	Fisher Scientific	Cat#: R91450001G, CAS: 7732-18-5
Critical commercial assays		
Pierce BCA Protein Assay Kit	ThermoFisher Scientific	Cat#: 23327
ATP Bioluminescence Assay Kit CLS II	Roche Diagnostics	Cat#: 11699695001
SuperSignal West Pico PLUS Chemiluminescent Substrate	Thermo Scientific	Cat#: 34580
iScript cDNA Synthesis Kit	BioRad	Cat#: 1708890
RNeasy Mini Kit	QIAGEN	Cat#: 74104
MitoSox Red Mitochondrial Superoxide Indicator	ThermoFisher Scientific	Cat#: M36008
Amplex red Hydrogen Peroxide/Peroxidase Assay Kit	ThermoFisher Scientific	Cat#: A22188
Homocysteine Fluorometric Kit	Abcam	Cat#: Ab228559
Seahorse XFe96 FluxPak	Agilent	Cat#: 102416-100
Seahorse XFe96 Cell Culture Microplate	Agilent	Cat#: 101085-004
Deposited data		
Mendeley Data	This study	https://doi.org/10.17632/djjv7tg4rv.1
Experimental models: Organisms/strains		
Caenorhabditis elegans (WT)	CGC	N2
dvIs100 [unc-54p::A-beta-1-42::unc-54 3′-UTR + mtl-2p::GFP] V	CGC	GMC101
smg-1(cc546) I; *dvIs27 [myo-3p::A-Beta (1-42)::let-851 3′UTR) + rol-6(su1006)]* X	CGC	CL4176
eat-2 (ad465) II; *dvIs100[unc-54p:: A-beta-1-42 + mtl-2p::GFP]* V	This study	UDE96
gcn-2(ok871) II; *dvIs100 [unc-54p::A-beta-1-42:: unc-54 3′UTR + mtl-2p::GFP]* V	This study	UDE90
dvIs100[unc-54p::A-beta-1-42::unc-54 3′UTR + mtl-2p::GFP] V; *pek-1(ok275)* X	This study	UDE21
foxSi16 [myo-3p::tomm-20:: mKate2::HA::tbb-2 3′ UTR] I	CGC	SJZ47
foxSi16 [myo-3p::tomm-20::mKate2::HA::tbb-2 3′ UTR] I; *dvIs100 [unc-54p::A-beta-1-42 + mtl-2p::GFP]* V	This study	UDE123
wwIs24 [acdh-1p::GFP + unc-119(+)]	CGC	VL749
dvIs100[unc-54p::A-beta-1-42::unc-54 3′UTR + mtl-2p::GFP] V; *pcca-1(ok2282)* X	This study	UDE148

(*Continued on next page*)

Version of record at: https://doi.org/10.1016/j.celrep.2021.109753

Continued

REAGENT or RESOURCE	SOURCE	IDENTIFIER
metr-1(ok521) II; *dvIs100 [unc-54p::A-beta-1-42:: unc-54 3′UTR + mtl-2p::GFP]* V	This study	UDE146
mmcm-1(ok1637) III; *dvIs100[unc-54p:: A-beta-1-42 + mtl-2p::GFP]* V	This study	UDE194
dvIs100[unc-54p::A-beta-1-42 + mtl-2p:: GFP] V; *sams-1 (ok2946)* X	This study	UDE205
rmIs133[unc-54p::Q40::YFP] I	CGC	AM141
rmIs290 [unc-54p::Hsa-sod-1 (127X)::YFP] IV	CGC	AM725
Oligonucleotides		
eat-2(ad465) II	*eat-2* forward: GCTCATTCGCACTGTTGAA TAACACTTATAGCGGTTTCT	Common Reverse: GTTACTTA AGGCGTACGAGCC
Wild type at *eat-2(ad465)* II locus	WT forward: GCTCATTCGCACTGTTGAATAACA CTTATAGC GGTTTCC	Common Reverse: GTTACTTA AGGCGTACGAGCC
gcn-2(ok871) II	*gcn-2* forward: GTGTTCACCGCTG AATCGG	Common Reverse: GACCACA TCCATCGCAACAC
Wild type at *gcn-2(ok871)* II locus	WT forward: GCAGTGTTCTTCGCCTTCTC	Common Reverse: GACCACA TCCATCGCAACAC
pek-1(ok275) X	*pek-1* forward: CTCTTGACAGCGTACTCG	Common Reverse: GCCAACA GTACATCGATG
Wild type at *pek-1(ok275)* X locus	WT forward: GACACCAATCTCAGCTGTAG	Common Reverse: GCCAACA GTACATCGATG
pcca-1(ok2282) X	*pcca-1* forward: CAGGTGAGGGTAATG GCATC	Common Reverse: GCTGGA GCCAAGTTCATC
Wild type at *pcca-1(ok2282)* X locus	WT forward: CCTGAAGACGAGTGTTCATC	Common Reverse: GCTGGA GCCAAGTTCATC
metr-1(ok521) II	*metr-1* forward: GAGGAGTCGACGTG CTTCTC	Common Reverse: CGTCCG ACAAAGGAAGGC
Wild type at *metr-1(ok521)* II locus	WT forward: GTCGTTGGAGAGCTGTTC	COMMON REVERSE: CGTCCGA CAAAGGAAGGC
mmcm-1(ok1637) III	*mmcm-1* forward: GATGGCATTCTTGG GACCAG	Common Reverse: GAGAGACGC GGAGCAAATGC
Wild type at *mmcm-1(ok1637)* III locus	WT forward: GAGAGACGCGGAG CAAATGC	Common Reverse: GAGAGAC GCGGAGCAAATGC
sams-1(ok2946) X	*sams-1* forward: GGAGAAATTACCT CCAAGGC	Common Reverse: GCGATAGC AGATGTGGCTGG
Wild type at *sams-1(ok2946)* X locus	WT forward: GGTCTCTACCCAACACTCTC	Common Reverse: GCGATAGC AGATGTGGCTGG
nuo-2 qRT-PCR primers	GTGCTGACTGGTTTGAGC	GACCTCGTTGTATCCCG
mev-1 qRT-PCR primers	GGACAGATCTACAAATCGGG	CTTGTTGCTCTTGTTCTGGC
cyc-1 qRT-PCR primers	CGACATTGCTTCTGTACG	CAGTCATGATTGTGTCAACG
nduo-1 qRT-PCR primers	GCCATCCGTGCTAGAAGAC	CAAATGGCGCCCGGTTAAG
act-2 qRT-PCR primers	GCGCAAGTACTCCGTCTGGATCG	GGGTGTGAAAATCCGTAAGGCAGA
Software and algorithms		
ImageJ	National Institutes of Health	https://imagej.nih.gov/ij/
Graph Pad Prism 9	GraphPad Software Inc.	https://www.graphpad.com/
Quantstudio6 Real-time PCR	Thermofisher Scientific	Cat: 4485694
ZEN 2.3 Digital Imaging System	Zeiss	https://www.zeiss.com/corporate/int/home.html?vaURL=www.zeiss.de/en

Version of record at: https://doi.org/10.1016/j.celrep.2021.109753

CellPress
OPEN ACCESS

RESOURCE AVAILABILITY

Lead contact

Further information and reagent requests should be directed to and will be fulfilled by the lead contact, Jessica Tanis (jtanis@udel.edu).

Materials availability

C. elegans strains generated from our studies will be provided upon request. The University of Delaware Material Transfer Agreement Request Webform will be completed when research materials are transferred to an outside party.

Data and code availability

All original data have been deposited at Mendeley Data and are publicly available as of the date of publication; DOI is listed in the key resources table.

This paper does not report original code.

Any additional information required to reanalyze the data reported in this paper is available from the lead contact upon request.

EXPERIMENTAL MODEL AND SUBJECT DETAILS

Nematode Culture

All *C. elegans* strains were maintained on nematode growth medium (NGM) at 20°C as described (Brenner, 1974). The wild-type strain was Bristol N2; all other strains used in this study can be found in the key resources table. *eat-2(ad465)* was detected with SuperSelective genotyping (Touroutine and Tanis, 2020); standard duplex PCR genotyping was used for all deletion mutants.

Bacterial Strains

Escherichia coli strains used in this study include OP50, HB101, HT115, and DA837. Bacterial cultures for assay plates were grown in LB overnight shaking at 37°C to an OD_{600} of 1.0 (Eppendorf BioPhotometer D30) and seeded onto NGM plates. All plates were dried for three days at room temperature and stored at 4°C before use. Relative amount of bacteria on seeded plates was measured by washing bacteria off plates with M9 buffer following a 24 hour temperature shift to 25°C and OD_{600} was measured using an Eppendorf BioPhotomer D30.

METHOD DETAILS

Aβ-induced Paralysis Assay

Animals were synchronized by a pulse egg lay for paralysis assays, however, we note that the dietary shift in paralysis was also observed with worms synchronized by bleaching or picking of late fourth larval stage (L4) animals to assay plates (not shown). Four adult animals were placed on 6 cm NGM plates seeded with different bacteria for 4 hours and then removed. The animals grew at 20°C and then were shifted to 25°C when the majority reached the late L4 stage, identified by a white crescent with black central dot at the vulva. Starting 12 to 20 hours post temperature upshift, depending on the genotype of the strain being assayed, the number of paralyzed and non-paralyzed animals were counted every two hours. Due to substantial acceleration of Aβ-induced paralysis in *pek-1* mutants, animals were assessed for movement every hour following temperature upshift until all paralyzed. To determine the impact of B_{12} post development, animals grown on OP50+B_{12} plates were transferred to B_{12}-free OP50 plates at the end of the L4 stage immediately prior to temperature upshift. For the inverse experiment, animals grown on B_{12}-free plates were transferred to B_{12} supplemented plates at the end of L4 stage. A minimum of three biological replicates were performed per *C. elegans* strain / bacterial condition. Data were used to generate Kaplan-Meier survival plots and determine median time to paralysis (GraphPad Prism 9).

Nutrient and Metabolite Supplementation

Nutrient supplemented plates for paralysis assays contained 10mM D(+)-glucose (Fisher Scientific), 0.3mM sodium homogamma linolenate (Nu-Chek Prep), 0.1mM or 0.3mM oleic acid (ThermoFisher Scientific),148nM or 740 nM methylcobalamin (Millipore Sigma), 1.34 mM, 6.7 mM, 13.4mM, or 67 mM L-methionine (Fisher Scientific), 1 mM, 10 mM, or 20 mM choline chloride (Millipore Sigma), and 15mM or 30 mM DL-Homocysteine (Millipore Sigma). Supplements were added to autoclaved NGM media at 55°C. Specific concentrations used for each supplementation experiment are indicated in the figures and legends. Some of these concentrations for glucose (Alcántar-Fernández et al., 2018), fatty acids (Deline et al., 2013), methylcobalamin (Revtovich et al., 2019), L-methionine (Wei and Ruvkun, 2020), homocysteine (Wei and Ruvkun, 2020), and choline (Walker et al., 2011) were used in prior *C. elegans* work; additional concentrations were used to determine dose-dependent effects for certain treatments. Plates were stored at 4°C. Fatty acid supplemented plates were covered with foil to prevent light oxidation. Plates were seeded with the different *E. coli* cultures (OD_{600} = 1.0) and dried for three days before use.

Version of record at: https://doi.org/10.1016/j.celrep.2021.109753

Mitochondrial imaging and analysis

Mitochondrial morphology was visualized by imaging *C. elegans* expressing RFP-tagged TOMM-20 (P*myo-3*::*tomm-20*::mKate2::HA::*tbb-2* 3′ UTR) 24 hours after temperature upshift of late L4 animals to 25°C. Animals were immobilized with 10 μM levamisole on 3% agar pads and Z stack images were obtained with a Zeiss LSM880 confocal microscope. Images were analyzed with ImageJ by drawing a ROI around muscles and using the script below to determine mitochondrial length. Values below 1 μm were excluded, then average branch length was calculated. Images from at least thirty animals were analyzed for each condition. The following script was used: run("Clear Results"); run("Median...," "radius=1.5"); run("Unsharp Mask...," "radius=2.5 mask=0.90"); setAutoThreshold("Li dark"); //run("Threshold..."); setOption("BlackBackground," true); run("Convert to Mask"); run("Skeletonize (2D/3D)");
run("Analyze Skeleton (2D/3D)," "prune=[shortest branch] prune_0 calculate show display"); run("Summarize");

Vitamin B_{12} reporter imaging

Images of P*acdh-1::gfp* expression were taken of adult animals, 24 hr post L4, that had been immobilized on 3% agarose pads with 10 μM levamisole. All images were collected under identical exposure conditions using a Zeiss AxioZoom V16 microscope with Axiocam 702 mono camera and ZEN 2.3 Digital Imaging System.

Nile Red Staining

Nile Red staining of fixed *C. elegans* was performed as previously described with modifications (Brooks et al., 2009). Synchronized populations of animals were raised on plates ± 0.3 mM oleic acid and then suspended in 1 mL of water 24 hr post L4. 50 μL of fresh 10% paraformaldehyde solution (Electron Microscopy Sciences) was added, and the worms were placed on a nutator for 1 hr at room temperature. The PFA solution was removed, 1 mL of 1 μg/mL Nile Red (Thermofisher Scientific) in 1x M9 was added, and the worms were incubated for 30 minutes at room temperature. After removal of the Nile Red solution, the animals were washed 1x with M9 and mounted on 3% agarose pads. Z stack images were obtained with a Zeiss LSM880 confocal microscope using identical settings.

ATP, ROS, and Homocysteine Quantification

Approximately 1000 first larval stage (L1) animals synchronized by bleaching were grown on 10 cm plates at 20°C. Once the animals reached late L4, plates were shifted to 25°C for 24 hours (Figure 2) or 18 hours (Figures 3 and 4). Animals were washed 3x with 1x M9 and sonicated on ice with Tris-EDTA buffer (100mM Tris, 4mM EDTA pH 7.75) using a model 150V/T Ultrasonic Homogenizer for 5 minutes, then centrifuged at 14,000 RPM for 15 minutes at 4°C. The supernatant was collected and moved to a fresh tube. ATP quantitation was performed with the ATP Bioluminescence Assay Kit CLS II (Roche Diagnostics) using a Glomax Multi-Detection System reader as described (Chaya et al., 2021). ATP was normalized to protein content measured with the Pierce BCA protein assay kit (ThermoFisher Scientific). Triplicate technical replicates were performed for each sample; at least four biological samples were assayed for each dietary condition.

For ROS quantification, animals were prepared as for ATP quantification except animals were sonicated on ice in M9 buffer. To normalize samples, the Pierce BCA protein assay kit was used to determine supernatant volume required for 25 μg of protein. Hydrogen peroxide levels were measured using 2′,7′-Dichlorofluorescein diacetate/H_2DCFDA (Sigma-Aldrich) as described (Yoon et al., 2018). Briefly 50 μL of 50 μM H_2DCFDA was added to normalized worm samples in black 96 well plates and incubated at room temperature for 6 hours before fluorescence was measured. The Amplex Red Hydrogen Peroxide/Peroxidase Assay Kit (Thermofisher Scientific) was also used to measure hydrogen peroxide levels. Superoxide levels were assessed with the MitoSox Red Mitochondrial Superoxide Indicator Kit (ThermoFisher Scientific) following manufacturers protocols. Fluorescence and absorbance values were measured using a Glomax Multi-Detection System. Triplicate technical replicates were performed for each sample; at least six biological samples were assayed for each dietary condition.

For homocysteine quantification, animals were prepared as for ROS quantitation. Homocysteine levels in supernatants containing 25 μg of protein were determined using the Homocysteine Assay Fluorometric Kit (Abcam) following manufacturer instructions. Fluorescence was measured with use of a Glomax Multi-Detection System. Triplicate technical replicates were performed for each sample; four biological samples were assayed for each condition.

Oxygen Consumption Rate Measurements

Oxygen consumption was determined using a Seahorse XFe96 Analyzer (Agilent) as described (Ng and Gruber, 2019) with some modifications. Compounds to be injected were made and pipetted into the sensor cartridge from the Seahorse XFe96 FluxPak (Agilent) as follows. 40 mM Carbonyl cyanide-p-trifluoromethoxyphenylhydrazone (FCCP; Millipore Sigma) stock was made from 10 mg FCCP in 984 μl DMSO and 25 μl aliquots were stored at −20°C. 25 μl of FCCP stock was diluted in 2475 μl M9 buffer immediately before use and 22 μl of this 400 μM FCCP was loaded into drug port A of the sensor cartridge for a final well concentration of 40 μM following injection. 800 mM sodium azide (Acros Organics) stock was made from 130 mg sodium azide in 2.5 mL dH_2O; 24 μl was loaded into drug port B of the sensor cartridge for a final well concentration of 80 mM following injection. Animals were grown as indicated for the ATP assays, then washed 3x with 1x M9 buffer 24 hours post 25°C temperature shift and diluted to ~1 worm/μl in M9. 20 μl of nematodes in M9 solution were pipetted into 180 μl of M9 buffer. 10-18 animals in a total volume of 200 μl was the target number of nematodes for each well of a Seahorse XFe96 Cell Culture Microplate; four blank wells without animals were left for background correction.

Version of record at: https://doi.org/10.1016/j.celrep.2021.109753

Basal respiration measurements were conducted for 6 loops, then FCCP was injected and maximal respiration was measured for 6 loops, followed by sodium azide injection and non-mitochondrial oxygen consumption was measured for 6 loops. Each loop consisted of mix for 3 minutes, wait for 2 minutes, measure for 3 minutes. Data analysis was performed on wells with than contained 10-18 animals similar to previously described (Koopman et al., 2016). Basal respiration was calculated by averaging oxygen consumption rate (OCR) from loops 3-6 then subtracting non-mitochondrial oxygen consumption as determined from loop 18, the last measurement following sodium azide addition. Maximal respiration was determined following FCCP injection by averaging OCR from loops 9-11, then subtracting non-mitochondrial OCR from loop 18. For each well, basal and maximal OCR were divided by the number of animals in that well and are presented as pmol O_2/min/worm. Spare capacity was determined by subtracting basal from maximal OCR. Three independent assays were conducted over different days; at least 18 wells were analyzed per strain / diet.

Western Blotting

Eggs from gravid adults were isolated by bleaching and allowed to hatch rocking in M9 buffer overnight. Approximately 1000 starved L1s were pipetted onto each plate the following day. Plates were moved to 25°C when a majority of animals were late L4 and 24 hours later, worms were washed 3x with M9 and the pellet was flash frozen. 100 μL lysis buffer (100mM NaCl, 100mM Tris pH 7.5, 1% NP-40) supplemented with an EDTA-free Protease Inhibitor cocktail tablet (Roche) was added to the pellet, sonicated on ice (Model 150V/T Ultrasonic Homogenizer), and centrifuged 15 minutes at 4°C. The supernatant was transferred to a new tube and 20 μL was set aside for protein quantification (Pierce BCA protein assay kit). 2x protein sample buffer (80 mM Tris-HCl, 2% SDS, 10% glygerol, 0.0006% Bromophenol blue with 10% β-meracaptoethanol and 8M Urea) was added to the supernatant. Samples were heated at 55°C for 5 minutes and 30 μg of protein per sample was run on Tris-Tricine 16.5% precast polyacrylamide gels (BioRad) for Aβ or 10% Tris-Glycine (TGX) precast protein gels (BioRad) for NUO-2. Samples were transferred onto 0.2 μm (Aβ) or 0.45 μm (NUO-2) nitrocellulose membranes (Bio-Rad) for 40 minutes at 70V. Membranes were blocked in 5% non-fat milk in TBS with 0.1% Tween-20 one hour at room temperature. Primary antibody incubation was overnight at 4°C; Aβ (6E10 Biolegend cat#803001, 1:1000), NUO-2 (Abcam cat#ab14711, 1:5000), and α-tubulin (Sigma cat#T9026, 1:5000) antibodies were used. Incubation with a goat anti-Mouse IgG-HRP (ThermoFisher Scientific cat#31430, 1:5000) secondary antibody conjugated to horseradish peroxidase was 1 ½ hr. at room temperature. Chemiluminescence detection used SuperSignal West Pico PLUS (ThermoFisher Scientific) and a Chemidoc MP Imaging System (BioRad). NUO-2 and the α-tubulin loading control were detected together on the same membrane, however, Aβ membranes had to be stripped and re-probed with the loading control antibody to ensure equal protein loading across gels. All experiments were done with five biological replicates.

qRT-PCR

C. elegans were synchronized as described for western blotting. 24 hr after temperature upshift, animals were washed three times with M9 and one time with non-DEPC treated RNase free water (Fisher Scientific), then transferred to a microcentrifuge tube. 400 μL of Trizol (ThermoFisher Scientific) was added and samples were flash frozen. RNA was isolated using the RNeasy Mini Kit (QIAGEN). Briefly, 200 μL of Trizol was added to thawed samples along with 140 μL of chloroform (ThermoFisher Scientific). Samples were centrifuged, the aqueous layer was removed, and equal volume of 70% ethanol was added. RNeasy spin columns (Quiagen) were used for on-column DNase treatment. Total RNA was transcribed into cDNA using the iScript cDNA Synthesis kit (BioRad). qRT-PCR was performed with PowerUp SYBR Green Master Mix (Applied Biosystems) using a Quantstudio 6 Flex Real-time PCR System (ThermoFisher Scientific) following the standard cycling mode with an anneal/extend temperature at 58°C followed by a default dissociation step. *act-2* was used as the housekeeping reference. The $\Delta\Delta C_t$ method was used to determine relative expression. Triplicate technical replicates were performed for each sample; data presented are from at least three biological replicates per condition.

Pharyngeal Pumping Rate Measurements

Animals were grown at 20°C to early L4 stage. Using the Zeiss AxioZoom V16 microscope the number of pharyngeal pumps per 30 s was counted. At least 25 animals were measured per diet.

Thrashing assay

Motility was assessed by quantitating thrashing rate in liquid. The wild-type was compared to animals expressing either a mutated form of human SOD-1 or a polyglutamine expansion transgene 24 hours post L4 on day 1 of adulthood. Nematodes were individually placed into a 10 μl drop of M9 buffer on a microscope slide and allowed to acclimate for 1 minute. The number of body bends completed in 1 minute was determined for 15 animals per strain / condition.

Preparation of Figures

Main text and supplemental figures were made with Adobe Illustrator; the graphical abstract was created with BioRender.com.

QUANTIFICATION AND STATISTICAL ANALYSIS

Data were analyzed with one-way ANOVA, performing multiple comparisons with the Dunnett test except where otherwise noted. Statistical analyses and graphing were performed with GraphPad Prism 9. Significant differences are indicated as $^{*}p < 0.05$, $^{**}p < 0.01$, $^{***}p < 0.001$, $^{****}p < 0.0001$.